Molecular Basis of the Interaction of the Human Protein Tyrosine Phosphatase Non-receptor Type 4 (PTPN4) with the Mitogen-activated Protein Kinase p38γ

Pierre Maisonneuve, Celia Caillet-Saguy, Marie-Christine Vaney, Edoo Bibi-Zainab, Kristi Sawyer, Bertrand Raynal, Ahmed Haouz, Muriel Delepierre, Monique Lafon, Florence Cordier, et al.

THE JOURNAL OF BIOLOGICAL CHEMISTRY VOL. 291, NO. 32, pp. 16699–16708, August 5, 2016

Molecular Basis of the Interaction of the Human Protein Tyrosine Phosphatase Non-receptor Type 4 (PTPN4) with the Mitogen-activated Protein Kinase p38γ*

Received for publication, December 1, 2015, and in revised form, April 6, 2016 Published, JBC Papers in Press, May 31, 2016, DOI 10.1074/jbc.M115.707208

Pierre Maisonneuve[‡§¶1], Célia Caillet-Saguy[‡§2], Marie-Christine Vaney[‖], Edoo Bibi-Zainab[‡§], Kristi Sawyer[‡§3], Bertrand Raynal[§‡‡], Ahmed Haouz[§¶¶], Muriel Delepierre[‡§], Monique Lafon[**§§], Florence Cordier[‡§], and Nicolas Wolff[‡§4]**

From the [‡]Département de Biologie Structurale et Chimie, Unité de Résonance Magnétique Nucléaire des Biomolécules, [‖]Unité de Virologie Structurale, Département de Virologie, [§§]Unité de Neuro-Immunologie Virale, Département de Virologie, [‡‡]Plate-Forme de Biophysique des Macromolécules, and [¶¶]Plate-Forme de Cristallographie, Institut Pasteur, F-75724 Paris, France, [§]UMR 3528 and [**]UMR 3569, CNRS, F-75724 Paris, France, and [¶]Université Pierre et Marie Curie, Cellule Pasteur UPMC, 75005 Paris, France

The human protein tyrosine phosphatase non-receptor type 4 (PTPN4) prevents cell death induction in neuroblastoma and glioblastoma cell lines in a PDZ·PDZ binding motifs-dependent manner, but the cellular partners of PTPN4 involved in cell protection are unknown. Here, we described the mitogen-activated protein kinase p38γ as a cellular partner of PTPN4. The main contribution to the p38γ·PTPN4 complex formation is the tight interaction between the C terminus of p38γ and the PDZ domain of PTPN4. We solved the crystal structure of the PDZ domain of PTPN4 bound to the p38γ C terminus. We identified the molecular basis of recognition of the C-terminal sequence of p38γ that displays the highest affinity among all endogenous partners of PTPN4. We showed that the p38γ C terminus is also an efficient inducer of cell death after its intracellular delivery. In addition to recruiting the kinase, the binding of the C-terminal sequence of p38γ to PTPN4 abolishes the catalytic autoinhibition of PTPN4 and thus activates the phosphatase, which can efficiently dephosphorylate the activation loop of p38γ. We presume that the p38γ·PTPN4 interaction promotes cellular signaling, preventing cell death induction.

PTPN4[5] is a non-receptor-tyrosine phosphatase (PTP) with functions in T cell signaling, learning, spatial memory, and cerebellar synaptic plasticity (1–3). Its overexpression reduces cell proliferation in COS-7 cells and suppresses CrkI-mediated cell growth and mobility in HEK293T cells (4, 5). PTPN4 also regulates neuronal cell homeostasis by protecting neurons against apoptosis (5, 6). PTPN4 is a large modular protein containing three domains, an N-terminal FERM domain, a PDZ domain, and a C-terminal catalytic tyrosine phosphatase domain (7). PDZ domains are protein-protein interaction domains, which play a central role in cell signaling by favoring spatial contacts between enzymes and their substrates or, more generally, by assembling and/or regulating protein networks (8, 9). Thus, disrupting the interactions between PDZ domains and PDZ binding motifs (PBM) can trigger profound alterations in cell signaling pathways (10–12). Such disruptions of PDZ·PBM complexes are used by viruses to hijack cell signaling pathways to their own advantage and can also be obtained by treating cells with an excess of cell penetrating peptide encoding a PBM (13). Indeed, we showed that rabies virus (RABV) peptides encoding a PBM can target the PDZ domain of PTPN4 (PTPN4-PDZ) and antagonize the function of PTPN4, leading to cell death (6). We optimized such pro-apoptotic peptides and designed the Cyto8-RETEV sequence, that is so far the most affine ligand of PTPN4-PDZ and the best inducer of cell death (15).

Four endogenous partners of PTPN4 have been reported: the glutamate receptor δ2 and ϵ subunits, the T-cell receptor ξ subunit, the CrkI oncoprotein, and the TRIF (TIR domain-containing adaptor-inducing interferon-B)-related adaptor molecule TRAM (3, 5, 16, 17). Nevertheless, the natural ligands of PTPN4 involved in the regulation of cell homeostasis remain unknown. Hou *et al.* (12) have identified p38γ, a mitogen-activated protein kinase (MAPK), as an endogenous partner of PTPN3, the closest homologous protein of PTPN4. MAPKs, including extracellular signal-regulated kinases (ERK), c-Jun N-terminal kinases, and p38s, are a major class of kinases involved in signaling cascades that mediate and integrate signals for a coordinated cellular response such as proliferation, transformation, and cell death (18). p38γ is the only MAPK that encodes a PBM (KETPL) at its C terminus allowing interactions with PDZ domain-containing proteins. The RAS-dependent oncogenic activity of p38γ results from the direct interaction between the PBM of p38γ and the PDZ domain of PTPN3 (PTPN3-PDZ), which allows the catalytic domains of PTPN3 to dephosphory-

* This work was supported by TGIR-RMN-THC Fr3050 CNRS. The authors declare that they have no conflicts of interest with the contents of this article.

The atomic coordinates and structure factors (codes 5EYZ and 5EZ0) have been deposited in the Protein Data Bank (http://wwpdb.org/).

[1] Supported by grants from the Ministère de l'Enseignement Supérieur et de la Recherche and the Fondation pour la Recherche Médicale FDT20130927999.

[2] Recipient of a Bourse Roux postdoctoral fellowship from the Pasteur Institute.

[3] Supported by a student mobility grant through the Erasmus+ Programme.

[4] To whom correspondence should be addressed: Unité de RMN des biomolécules, Institut Pasteur, UMR 3528 CNRS, 28 rue du Dr Roux, 75724 Paris cedex 15. Tel.: 33-1-45-68-88-72; Fax: 33-1-45-68-89-29; E-mail: nicolas.wolff@pasteur.fr.

[5] The abbreviations used are: PTPN4, protein tyrosine phosphatase (PTP) non-receptor type 4; PDZ, PSD95 Dlg Zo-1; PBM, PDZ binding motif; RABV, rabies virus; HSQC, heteronuclear single quantum coherence; ITC, Isothermal calorimetry; TEV, tobacco etch virus; TCEP, tris (2-carboxyethyl)phosphine.

late a phosphotyrosine residue on p38γ (12). PTPN3 and PTPN4 are members of the NT5 non-receptor-tyrosine phosphatase group. They contain the same modular organization and have a high sequence identity of 71 and 65% for the PDZ and phosphatase domains, respectively. Thus, we surmised that p38γ could be a ligand of PTPN4-PDZ involved in PTPN4 cell signaling. Interestingly, silencing PTPN4 or p38γ genes is phenotypically equivalent and results in massive cell death (19). A similar phenotype is also observed when PTPN4-PDZ is targeted by peptides encoding a PBM after their intracellular delivery (15).

Here, we show that full-length p38γ and PTPN4-PDZ interact *in vitro* in GST pulldown assays. The C-terminal sequence of p38γ (p38γ-KETPL), encompassing the PBM, interacts tightly with PTPN4-PDZ and has the highest affinity of all endogenous PTPN4 ligands. NMR and x-ray structural data of the PTPN4-PDZ and p38γ-KETPL complex and of the PTPN4-PDZ and optimized peptide Cyto8-RETEV complex lead us to identify the structural basis for PBM recognition by PTPN4-PDZ. We also highlight the predominant role of this PDZ·PBM association in the molecular interactions between the full-length p38γ and the physiologically active PTPN4 two-domain (PDZ-PTP) encompassing the PDZ and the phosphatase domains. As a functional consequence, the binding of p38γ-KETPL to PTPN4-PDZ lifts the auto-inhibited state of PTPN4 and activates the phosphatase. Finally, the peptide p38γ-KETPL efficiently promotes death of human glioblastoma upon intracellular delivery.

Experimental Procedures

Production of Recombinant Proteins and PBM Ligands—p38γ is cloned in a pET15b expression plasmid and is encoded as an N-terminal 6-histidine (His)-tagged protein. Uniformly ^{15}N-labeled and non-labeled PTPN4 PDZ, PTP, PDZ-PTP^{WT}, and PDZ-PTP^{CS} constructs were expressed and purified as previously described (20). The unlabeled, ^{15}N-labeled and ^{13}C,^{2}H,^{15}N-labeled p38γ proteins were purified as previously described (20). PDZ ligands, p38γ-KETPL (SWARVSKETPL) and Cyto8-RETEV (SWESHKSGRETEV), were synthesized in solid phase using Fmoc (*N*-(9-fluorenyl)methoxycarbonyl) strategy (Proteogenix).

GST Pulldown Assay—GST fusion construct containing the PDZ domain of PTPN4 (GST-PTPN4-PDZ) was expressed and purified as previously described (15) without TEV cleavage. GST was purified after an additional TEV cleavage step of GST-PTPN4-PDZ. Purified GST-PTPN4-PDZ or GST was individually incubated with glutathione-agarose beads for 1 h at 4 °C with mild shaking. The beads were pelleted by centrifugation and washed 3 times with binding buffer (50 mM Tris-HCl, pH 7.5, 150 mM NaCl, 0.5 mM TCEP). Immobilized GST or GST-PTPN4-PDZ was incubated with mild shaking for 1 h at 4 °C with an equivalent ratio (v/v) of beads:lysate of human neuroblastoma cells (SH-SY5Y cells), which were prepared as previously described (6). Glutathione-agarose was washed four times and resuspended in a SDS-PAGE sample buffer. After boiling, the bound proteins were analyzed using 12% SDS-PAGE followed by Western blotting using anti-p38γ antibody (Cell Signaling, #2307) and Rabbit TrueBlot® monoclonal antibody (Rockland). The proteins were visualized by enhanced chemiluminescence according to the manufacturer's instructions (Amersham Biosciences).

Crystallization, Data Collection, and Structure Determination—The Cyto8-RETEV and p38γ-KETPL peptides used for co-crystallizations were added in excess to form >95% of the complex with the protein. PDZ domain·ligand complexes for crystallization were generated by mixing PTPN4-PDZ domain and the appropriate peptide at a ratio of 1:2 and 1:4 for PTPN4-PDZ·Cyto8-RETEV and PTPN4-PDZ·p38γ-KETPL, respectively, and incubating the mixture for 30 min on ice before crystallization experiments.

The crystals were obtained by vapor diffusion in sitting drops at 18 °C. An aliquot (400 nl) of PTPN4-PDZ·Cyto8-RETEV complex solution (concentration of the PDZ domain at 4.5 mg/ml) in 50 mM Tris-HCl, pH 7.5, 150 mM NaCl, 0.5 mM TCEP was mixed with 200 nl of well precipitant solution containing 23% PEG 8000, 100 mM MES, pH 6.0, 200 mM calcium acetate, 0.143 mM ammonium sulfate. An aliquot (200 nl) of PTPN4-PDZ·p38γ-KETPL complex solution (concentration of the PDZ domain at 5 mg/ml) in the same buffer with 200 nl of well precipitant solution containing 1.2 M sodium dihydrogen phosphate, 0.8 M dipotassium hydrogen phosphate, 0.1 M CAPS, pH 10.5, 0.2 M lithium sulfate, 0.67 M non-detergent sulfobetaine (NDSB) 201.

Crystals were then flash-cooled in liquid nitrogen using Paratone-paraffin (50%/50%) oil as the cryoprotectant. X-ray diffraction data were collected on beamline PROXIMA-1 at Synchrotron SOLEIL (St. Aubin, France). The data were processed with XDS (21), SCALA (22), and other programs from the CCP4 suite (23).

The structures were solved by molecular replacement with PHASER (24) using the search atomic model of PTPN4-PDZ (PDB access code 3NFK). The locations of the bound peptides were determined from a $F_o - F_c$ difference electron density map. Models were rebuilt using COOT (25), and refinement was performed using BUSTER (26). The overall assessment of model quality was performed using MolProbity (27). The crystal parameters, data collection statistics, and final refinement statistics are shown in Table 1. All structural figures were generated with the PyMOL Molecular Graphics System, version 1.5.0.4 (Schrödinger).

The asymmetric unit of PTPN4-PDZ·Cyto8-RETEV and PTPN4-PDZ·p38γ-KETPL crystal structures contains four subunits of protein·peptide complex. Each subunit corresponds to the complex formed by PTPN4-PDZ protein (chains A, B, C, and D) with the peptides (chains E, F, G, and H), respectively, A-E, B-F, C-G, and D-H. The four PTPN4-PDZ subunits are disulfide-bonded by pair: chains A to B and chains C to D for PTPN4-PDZ·Cyto8-RETEV structure; chains A to D and chains B to C for PTPN4-PDZ·p38γ-KETPL structure. However, the monomeric state of the PDZ domain in complex with these peptides in solution was previously confirmed, implying that the intermolecular disulfide bonds are due to crystalline conditions (15) and (20).

For the PTPN4-PDZ·Cyto8-RETEV structure, only 6 C-terminal residues of the 13 residues of Cyto8-RETEV were well defined in the electronic density. For the PTPN4-PDZ·p38γ-

TABLE 1
Crystallographic and structure refinement statistics

Crystal	PTPN4·Cyto8-RETEV	PTPN4·p38γ-KETPL
PDB ID	5EYZ	5EZ0
Data collection[a]		
Space group	$C\,2\,2\,2_1$	$C\,2\,2\,2_1$
Unit cell (Å)		
a, b, c	77.7, 80.9, 170.2	68.5, 76.1, 198.7
α, β, γ (°)	90, 90, 90	90, 90, 90
Number of complex per asymmetric unit	4	4
Resolution range (Å)	46.80-2.09 (2.20-2.09)	49.35-2.35 (2.48-2.35)
Number of unique reflections	30,269 (2,870)	21,504 (2,967)
Completeness (%)	94.2 (63.0)	97.5 (93.7)
Multiplicity	4.7 (3.1)	4.6 (3.5)
R_{merge} (%)[b]	4.9 (50.8)	7.6 (49.7)
$\langle I/\sigma(I)\rangle$	14.2 (1.7)	12.7 (2.2)
Refinement		
R factor (%)[c]	22.91	22.52
R free (%)[d]	23.95	24.48
r.m.s.d. bond length (Å)[e]	0.007	0.007
Bond angle [°][e]	0.97	0.98
Ramachandran plot[f]		
Most favored (%)	96.8	96.6
Additional allowed (%)	2.6	3.1
Outliers (%)	0.52	0.26

[a] Values in parentheses refer to statistics in the highest resolution bin.
[b] $R_{merge} = \sum|(I - \langle I\rangle)/\sum(I)$.
[c] R factor = $\sum|F_{obs} - F_{calc}|/\sum F_{obs}$.
[d] R_{free} was calculated with 5% of the data excluded from the refinement.
[e] r.m.s.d., root mean square deviation from ideality.
[f] Categories were defined by MolProbity (14).

KETPL structure, in two subunits (chains A-E and B-F), only six C-terminal residues of p38γ-KETPL were well defined into the electronic density, whereas due to crystal packing in the other subunits (chains C-G and D-H), all of the 11 residues of p38γ-KETPL in chain G and H were well ordered. The four PDZ domains from each subunit of the asymmetric unit superimpose very well with a root mean square deviation on Cα of 0.17 Å and 0.33 Å for the PTPN4-PDZ·Cyto8-RETEV and PTPN4-PDZ·p38γ-KETPL complexes, respectively, indicating that crystal packing has no influence in the overall structure of the PDZ domain. In the following text, we described the PTPN4-PDZ·Cyto8-RETEV complex formed by the C and G chains and the PTPN4-PDZ·p38γ-KETPL complex formed by the D and H chains.

Peptide-induced Cell Death—Peptides were conjugated to the HIV-1 Tat domain and labeled with a FITC molecule as previously described (6). Human grade III U373MG glioblastoma cells (HTB 17; ATCC) (250,000 cells per well in 1 ml of culture medium) were treated with FITC-conjugated peptides at a concentration of 25 mM. Three hours post treatment, cells were assayed for peptide entry (FITC-positive cells), and cell death (propidium iodide-positive cells) was by flow cytometry (FACSCalibur, BD Biosciences) using the Cell Quest Pro software as described (15).

NMR Experiments—^{15}N-Labeled NMR samples of PTPN4-PDZ and of p38γ were prepared at concentrations of 220 mM in 250 ml of a buffer containing 50 mM Tris-HCl, pH 7.5, 150 mM NaCl, 0.5 mM TCEP, protease inhibitor mixture (Roche Applied Science), and 12% D_2O. Stock solutions of unlabeled PTPN4-PDZ and p38γ were prepared at concentrations of 540 μM in the same buffer. The ^{15}N-PTPN4-PDZ·unlabeled-p38γ complex was formed at 140:225 μM (1:1.6 molar ratio), and the ^{15}N-p38γ·unlabeled-PTPN4-PDZ complex was formed at 150:175 μM (1:1.2 molar ratio). All the ^{1}H,^{15}N HSQC spectra recorded on these samples to map the PTPN4-PDZ·p38γ interaction were acquired at 25 °C on a Varian Inova 600-MHz spectrometer equipped with a cryoprobe, with 128 (60 ms) and 1024 (95 ms) complex points (acquisition times) in ^{15}N and ^{1}H, respectively.

The NMR titration experiment to measure the PTPN4-PDZ·p38γ-KETPL peptide affinity at 25 °C was performed as previously described (6). Briefly, the unlabeled p38γ-KETPL peptide (stock solution of 6.5 mM) was added stepwise in a sample initially containing 280 μl of ^{15}N-labeled PTPN4-PDZ at a concentration of 132 μM to a final PDZ/peptide ratio of 1:12 (final peptide concentration of 1.25 mM). A series of ^{1}H,^{15}N HSQC spectra was recorded for 10 different titration points.

The three-dimensional triple resonance NMR experiments for backbone resonance assignment of p38γ (HNCO, HN(CA)CO, HNCACB, HNCA, and HN(CO)CACB) were recorded at 25 °C on a Bruker 950 MHz spectrometer equipped with a cryoprobe, on a ^{13}C,^{2}H,^{15}N-labeled sample of p38γ prepared at a concentration of 380 μM in 180 μl of a buffer containing 50 mM Tris-HCl, pH 7.5, 150 mM NaCl, 0.5 mM TCEP, protease inhibitor mixture (Roche Applied Science), and 12% D_2O.

Isothermal Titration Calorimetry (ITC)—ITC experiments were performed with an ITC-200 (MicroCal) at 25 °C in a buffer of 50 mM Tris-HCl, pH 7.5, 150 mM NaCl, and 0.5 mM TCEP. PTPN4 construct concentration was initially 30.0 μM in the cell, whereas p38γ-KETPL peptide or p38γ protein concentrations in the syringe were 300 μM. For the competition experiments, the initial concentration of the p38γ-KETPL peptide in the cell was 150 μM. 16 aliquots of 2.4 μl of peptide were injected from the 40-μl syringe into the 200-μl cell, leaving an interval of 180 s between injections. The enthalpy of binding (Δ*H*), affinity constant (K_a), and molar binding stoichiometry (*N*) were determined by performing nonlinear curve-fitting of the corrected data to a model with one set of sites with Origin7.0 software (OriginLab).

Phosphorylation of p38γ—To generate phosphorylated p38γ for enzymatic assays, a p38γ sample at 100 μM was mixed at a molar ratio of 1:4000 of MKK6-EE·p38γ in a buffer composed of 250 mM Tris-HCl, pH 7.5, 125 mM NaCl, 0.4 mM TCEP, 5 mM $MgCl_2$, 5 mM MnCl2, 2 mM ATP. The mixture was incubated overnight at 22 °C. After incubation, the samples were purified by an ion-exchange column (HiPrep Q HP) and then eluted with a NaCl gradient. p38γ phosphorylation was controlled by electrospray ionization mass spectrometry.

Phosphatase Assay and Kinetic Analysis—Phosphatase activity with phosphopeptides and *p*-nitrophenyl phosphate was measured as previously described (20). Reactions were measured with various phosphopeptide pTGpY concentrations ranging from 1.8 μM to 225 μM at an enzyme concentration of 10 nM. The k_{cat} and K_m constants were deduced from fitting the Michaelis-Menten equation with the Origin software. The equation takes into account excess-substrate inhibition. The phosphatase activity using purified phospho-p38γ as a substrate was measured over 240 s with 1 point/s with 10 nM PTPN4-PDZ-PTP^{WT} with or without p38γ-KETPL peptide (final concentration 40 μM) or with linker-PTP and 30 μM

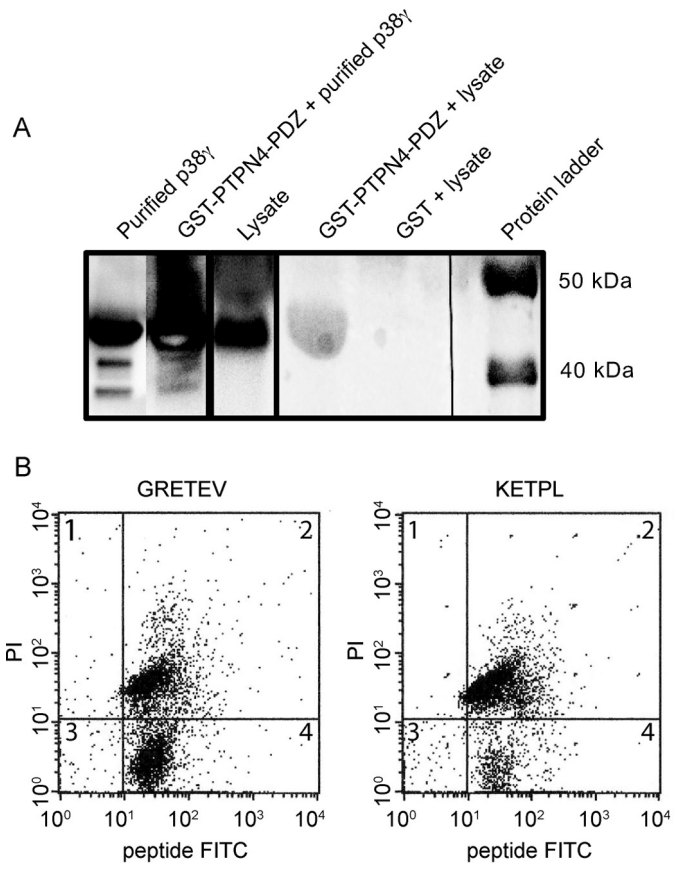

FIGURE 1. **Interaction between PTPN4-PDZ and endogenous p38γ and killing efficiency of the cell-penetrating PBM of p38γ.** *A*, GST pulldown assay demonstrating *in vitro* binding between PTPN4-PDZ and p38γ. The *first lane* shows the signal from purified p38γ. Immobilized GST-PTPN4-PDZ was mixed with purified p38γ in the *second lane*. The *third lane* shows the signal of endogenous p38γ in SH-SY5Y cell lysate. The *fourth lane* shows the signal from immobilized GST-PTPN4-PDZ mixed with cell lysate. The control of immobilized GST mixed with SH-SY5Y lysate is shown in the *fifth lane*. The protein ladder is shown in the *sixth lane*. The membrane is revealed with a p38γ antibody. *B*, glioblastoma cells U373MG were loaded with TAT and FITC conjugated GRETEV (*left*) or KETPL peptide (*right*). After 3 h in culture at 37 °C, dead cells (propidium iodide-positive cells localized in *quadrants 1* and *2*) and peptide-loaded cells (FITC-positive cells localized in *quadrants 2* and *4*) were measured by flow cytometry. GRETEV and KETPL peptides triggered death in 56 and 74% of peptide-loaded cells, respectively. In non-treated cells, the percentage of propidium iodide-positive cells was 3–5% (data not shown). These results are representative of three distinct experiments.

phospho-p38γ or TGpY peptide in the final volume and in buffer conditions identical to that of the phosphopeptide assay.

Results

A Direct Interaction between PTPN4-PDZ and Endogenous p38γ Is Detected by GST Pulldown Assays Using Neuroblastoma Cell Extracts—To identify a potential interaction between endogenous p38γ and PTPN4 through their PBM and PDZ, respectively, we performed pulldown analyses using human neuroblastoma SH-SY5Y cell lysates. The presence of p38γ was initially verified in cell lysate (Fig. 1*A*). Purified GST-PTPN4-PDZ and GST alone were incubated with the soluble fraction of SH-SY5Y cell lysates. As shown in Fig. 1*A*, endogenous p38γ binds to GST-PTPN4-PDZ but not to GST alone (Fig. 1*A*). The direct interaction was also confirmed with purified recombinant p38γ mixed with glutathione-agarose bound to GST-PTPN4-PDZ fusion proteins (Fig. 1*A*). Thus, the results demonstrate the direct interaction between endogenous p38γ and PTPN4-PDZ in cell lysates and suggest that p38γ is a physiological partner of PTPN4 through PDZ-mediated interaction.

PBM of p38γ Has a High Affinity for PTPN4-PDZ—The affinity of the PBM of p38γ (p38γ-KETPL peptide) for PTPN4-PDZ was measured by NMR titration. $^{1}H,^{15}N$ chemical shift perturbations of the PDZ domain were followed as a function of increasing concentrations of the p38γ-KETPL peptide to determine the dissociation constant (K_d). The p38γ-KETPL peptide binds to PTPN4-PDZ with a K_d of 1.58 ± 0.97 μM (Table 2). This affinity is very close to that of the Cyto8-RETEV sequence (K_d of 1.0 μM), which we have previously designed on structural basis to optimize PTPN4-PDZ binding (15). The C-terminal sequence of p38γ has the strongest affinity for PTPN4-PDZ compared with the two endogenous partners, GluN2A and GluD2, with K_d values of 42 μM and 128 μM, respectively.

PBM of p38γ and the Optimized Peptide Have a Similar Binding Mode to PTPN4-PDZ—To investigate the interaction of PTPN4-PDZ with the endogenous ligand p38γ-KETPL or the optimized ligand Cyto8-RETEV, the crystal structures of the two complexes were solved by molecular replacement at 2.35 Å and 2.09 Å resolutions, respectively (Table 1). The structure factors and coordinates for the structures PTPN4/Cyto8-RETEV and PTPN4/p38γ-KETPL have been deposited in the Protein data Bank under accession codes 5EYZ and 5EZ0, respectively.

The structures of PTPN4-PDZ·Cyto8-RETEV and PTPN4-PDZ·p38γ-KETPL are very similar with a root mean square deviation of 0.22 Å. PTPN4-PDZ adopts the typical PDZ fold comprising five β-strands and two α-helices (Fig. 2*A*) and possesses the interaction network specific to class I PDZ domains that recognize the consensus peptide sequence X(S/T)$X\Phi_{COOH}$, where X is any residue, and Φ is a hydrophobic residue. The last six C-terminal residues encompassing the PBM of Cyto8-RETEV (-GRETEV$_{-COOH}$) and p38γ-KETPL (-SKETPL$_{-COOH}$) are well ordered in the crystal. The peptides were inserted into the PDZ-binding pocket in the conventional mode (Fig. 2). The interactions of the residues at the positions 0, −2, and −3 of both peptides with PTPN4-PDZ are quite similar to the bonding patterns already observed in the complex between PTPN4-PDZ and the viral peptide Cyto13-att (-GETRL$_{-COOH}$) (x-ray structure PDB code 3NFK; Ref. 15). The peptide Cyto13-att corresponds to the last 13 residues of the G envelope protein from an attenuated RABV strain. Starting from the Cyto13-att sequence that binds PTPN4-PDZ with a K_d of 157 μM, the Cyto8-RETEV sequence has been optimized focusing on the residues at positions −1 (Arg → Glu) and −4 (Gly → Arg). These positions are not involved in the network of interactions between the viral sequence and PTPN4-PDZ (15). Here, we confirm our previous postulate that Glu at position −1 and Arg at position −4 in Cyto8-RETEV likely induces crucial polar contacts with the surrounding residues of PTPN4-PDZ and consequently improve the affinity for PTPN4-PDZ.

The cationic side chain at position −1 in the viral peptide Cyto13-att (-GETRL$_{-COOH}$) is unfavorable in the positively charged environment of PTPN4-PDZ consisting of residues Arg-527, Arg-546, and Lys-587. The acidic residue (Glu) in Cyto8-RETEV and the neutral residue (Pro) in p38γ-KETPL at

TABLE 2

Constants of dissociation and thermodynamic parameters of p38γ binding with different PTPN4 constructs

K_d was measured using ITC at 25 °C with PTPN4 constructs at a concentration of 30 μM in 50 mM Tris, pH 7.5, 150 mM NaCl, 0.5 mM TCEP·p38γ-KETPL peptide was added at 150 μM for the last experiment. N corresponds to the stoichiometry, and ΔH and $T\Delta S$ correspond to the enthalpy and entropy of the system, respectively. (K_d measured by NMR titration).

p38γ constructs	Cell titration	PTPN4 constructs	N	K_d	ΔH	$-T\Delta S$	ΔG
				μM	*kcal/mol*	*kcal/mol*	*kcal/mol*
p38γ-KETPL	Buffer	PDZ		1.58 ± 0.97			
p38γ-KETPL	Buffer	PDZ-PTP$^{C/S}$	0.88 ± 0.02	1.54 ± 0.24	−6.92 ± 0. 18	−1.00 ± 0.44	−7.93 ± 0.13
p38γ	Buffer	PDZ-PTP$^{C/S}$	0.90 ± 0.01	4.10 ± 0.28	−7.93 ± 0.16	0.58 ± 0.31	−7.35 ± 0.06
p38γ	p38γ-KETPL	PDZ-PTP$^{C/S}$	No titration				

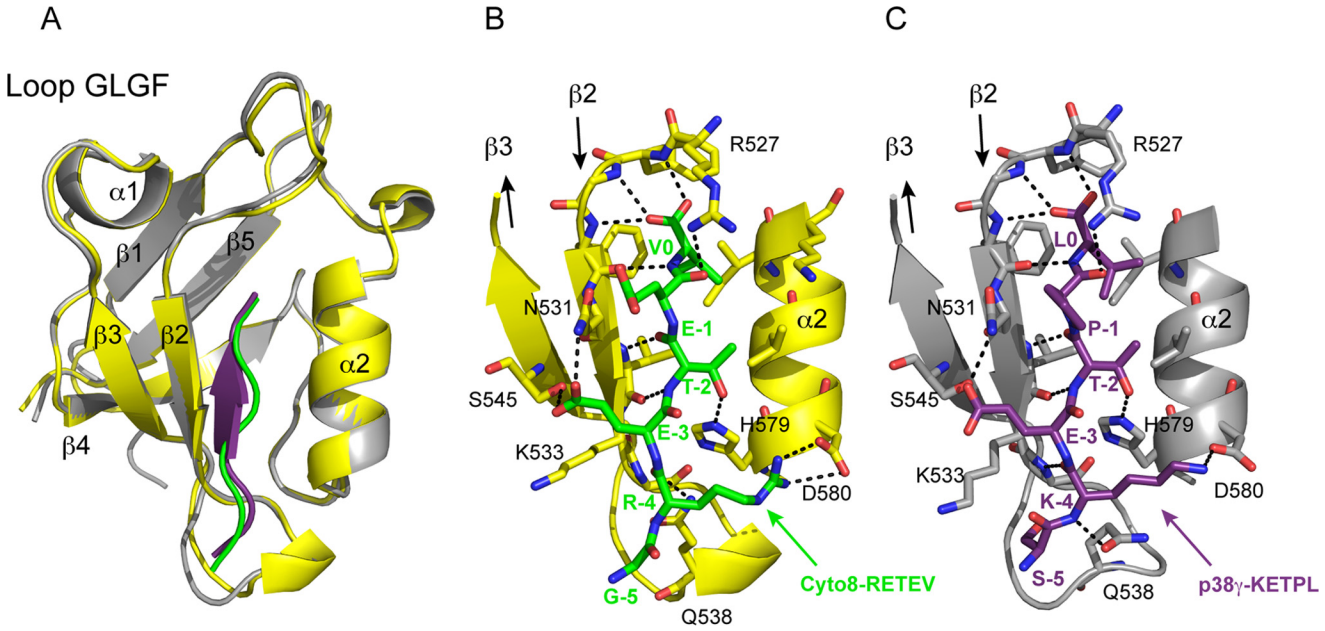

FIGURE 2. **Structure of PTPN4-PDZ bound to Cyto8-RETEV and p38γ-KETPL.** *A*, superposition of PTPN4-PDZ bound to Cyto8-RETEV (*yellow* and *green*, respectively) and p38γ-KETPL (*gray* and *purple*, respectively). Peptides bind to the PDZ domain through a canonical mode in the PDZ binding site delimited by the β2 strand, α2 helix, and the GLGF loop. *B* and *C*, close-up views of the PTPN4-PDZ/peptide binding sites. Important residues are shown as *sticks* in Corey-Pauling-Koltun colors. Peptides form an antiparallel β sheet with the β2 strand via a complete set of intermolecular canonical backbone H-bonds. All H-bonds between PTPN4-PDZ and peptides are indicated by *black dashed lines*. Color coding for PTPN4-PDZ and peptides is the same as *A*.

position −1 are fully exposed to the solvent. However, these residues are H-bonded to PTPN4-PDZ involving the oxygen atom of their peptidic bond and the Hζ of the Arg-527 from the PTPN4-PDZ binding site GLGF loop (Fig. 2, *B* and *C*). The basic side chains at position −4, Arg for Cyto8-RETEV and Lys for p38γ-KETPL, form a H-bond with the Cγ carboxyl oxygen of the Asp-580 located at the bottom of the α-helix 2. These additional interactions could mainly explain the increase in binding free energy of complex formation with Cyto13-att compared with Cyto8-RETEV or p38γ-KETPL ($\Delta\Delta G_0$ = RTln(K_D(Cyto13-att)/K_D(Cyto8-RETEV)) = 2.8 kcal·mol^{-1} or $\Delta\Delta G_0$ = RTln(K_D(Cyto13-att)/K_D(p38γ-KETPL)) = 2.7 kcal·mol^{-1}) corresponding to a 160-fold and 100-fold difference in affinity, respectively. Thus, similar binding modes of p38γ-KETPL and Cyto8-RETEV with PTPN4-PDZ are found for the key positions of recognition between PBM and PDZ, explaining the similar strong affinity of p38γ-KETPL and Cyto8-RETEV for PTPN4-PDZ.

PBM of p38γ Is an Efficient Inducer of Cell Death in Human Glioblastoma Cell Line Expressing PTPN4—The affinities of PBM peptides for PTPN4-PDZ are closely correlated to their killing efficiency after their intracellular delivery (15). We conceived the best-suited Cyto8-RETEV peptide that binds with the highest affinity to PTPN4-PDZ and consequently the best inducer of cell death. In the same way, the killing efficiency of the Tat-conjugated peptide of the C-terminal PBM of p38γ was estimated in U373MG (Fig. 1*B*), a human glioblastoma cell line expressing PTPN4. After a 3-h exposure of U373MG to the peptide, a delay sufficient for maximal peptide entry, the induction of cell death was measured by propidium iodide assay. A 2-fold increase of glioblastoma cell death was observed using p38γ-KETPL compared with Cyto8-RETEV with a similar capacity to enter the cells for both peptides. Thus, p38γ-KETPL is an efficient inducer of cell death in glioblastoma.

Mapping the PTPN4-PDZ·p38γ Interaction in Vitro—To investigate the molecular basis of the interaction between p38γ and PTPN4, we probed *in vitro* the binding of PTPN4-PDZ to full-length p38γ by NMR chemical shift perturbation experiments on both sides of the partners. ^{1}H,^{15}N HSQC spectra were recorded on ^{15}N-labeled PTPN4-PDZ in its free form, in the presence of unlabeled p38γ-KETPL peptide and in the presence of unlabeled p38γ full-length protein.

The addition of p38γ-KETPL peptide induces strong ^{1}H,^{15}N chemical shift changes on PTPN4-PDZ (Fig. 3*A*). Residues on strands β2, β3, and helix α2 are the most affected by the binding ($\Delta\delta_{avg} > 0.17$ ppm) (Fig. 3, *B* and *C*), suggesting a conventional

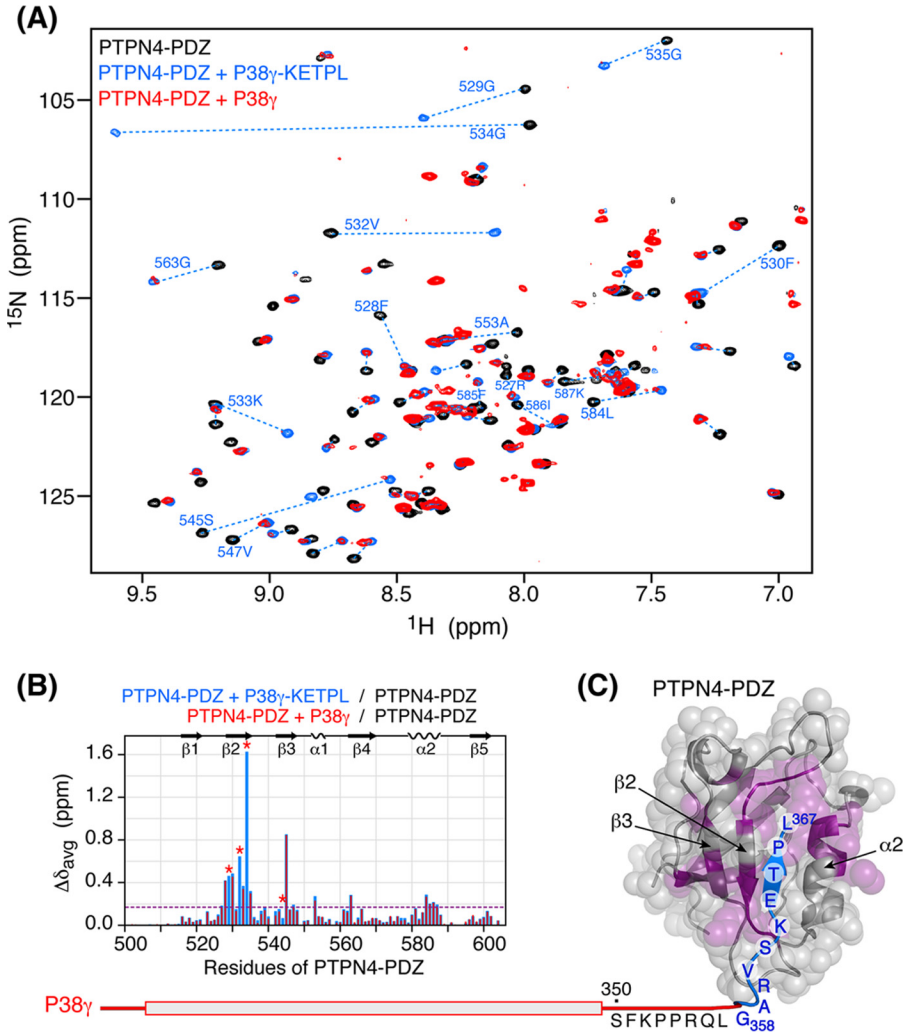

FIGURE 3. **Mapping of the PTPN4-PDZ·p38γ interaction by NMR chemical shift perturbations.** *A*, chemical shift perturbations of PTPN4-PDZ upon binding to p38γ: overlay of $^{1}H,^{15}N$ HSQC spectra recorded on free PTPN4-PDZ (*black*), on PTPN4-PDZ in complex with p38γ-KETPL peptide (*blue*), and on PTPN4-PDZ in complex with full-length p38γ (*red*). The large chemical shift changes are indicated by *dotted blue lines*. Assignment is indicated for the most affected residues ($\Delta\delta_{avg} > 0.17$ ppm; see in *B*). *B*, $^{1}H,^{15}N$-weighted average chemical shift differences $\Delta\delta_{avg}$ between PTPN4-PDZ and PTPN4-PDZ·p38γ-KETPL complex (*blue*) and between PTPN4-PDZ and PTPN4-PDZ·p38γ complex (*red*), calculated as $\Delta\delta_{avg} = (\Delta\delta H^2 + (\Delta\delta N \times 0.159)^2)^{1/2}$. The *red asterisks* denote residues for which no resonance peaks were detected in the PTPN4-PDZ·p38γ complex due to exchange broadening. Secondary structure elements are indicated at the *top*. *C*, structure of PTPN4-PDZ (*gray ribbon* and *space-fill representations*) bound to p38γ-KETPL peptide (*blue ribbon*) showing the same binding surface of p38γ-KETPL peptide or full-length p38γ onto PTPN4-PDZ (in *violet*), as identified by the large NMR chemical shift perturbations in *B*: $\Delta\delta_{avg} > 0.17$ ppm. The p38γ residues, the most affected by PTPN4-PDZ binding (Fig. 4), are shown in *blue* (Gly-358–Leu-367$_{COOH}$). The full-length p38γ until the −7 position of the PBM is schematic.

anchoring mode of the PBM into the PDZ groove. Overall, the same chemical shift perturbations are observed by the addition of full-length p38γ (Fig. 3, *A* and *B*). Four resonance peaks were severely affected by exchange broadening and not detected in the spectrum and corresponded to residues localized near the binding groove. Thus, the same surface was mapped on PTPN4-PDZ by the binding of the short p38γ-KETPL peptide or of the full-length p38γ protein (Fig. 3*C*).

We compared $^{1}H,^{15}N$ HSQC spectra recorded on ^{15}N-labeled full-length p38γ in its free form and in the presence of unlabeled PTPN4-PDZ to map the residues of the kinase perturbed by the interaction with PTPN4-PDZ (Fig. 4). Backbone assignment of p38γ was performed on a $^{13}C,^{2}H,^{15}N$-labeled sample using a set of three-dimensional heteronuclear NMR experiments recorded at 950 MHz. Over the 349 expected non-proline residues, 273 amide signals were visible in the HSQC spectrum and only 154 could be assigned (44.1%) (Fig. 4) (BMRB (Biological Magnetic Resonance Bank) accession number 26758). Note that similar results were previously obtained for the homologous MAP kinase p38α (28) for which 64% of amide signals were initially assigned using a set of selectively ^{15}N-labeled samples and distance information from a paramagnetic adenosine derivate. Later, the sequence-specific backbone assignment was improved to 82% (29). Our partial assignment of p38γ is sufficient to unambiguously identify residues perturbed by the binding of PTPN4-PDZ as the C terminus residues from Gly-358 to Leu-367$_{COOH}$. In the presence of PTPN4-PDZ, the latter were essentially affected by exchange broadening, and this line broadening increased in a gradual manner toward the C terminus (from Gly-358 to Leu-367), up to the complete disappearance of Thr-365 and Leu-367 resonances (Fig. 4). These results indicate that full-length p38γ

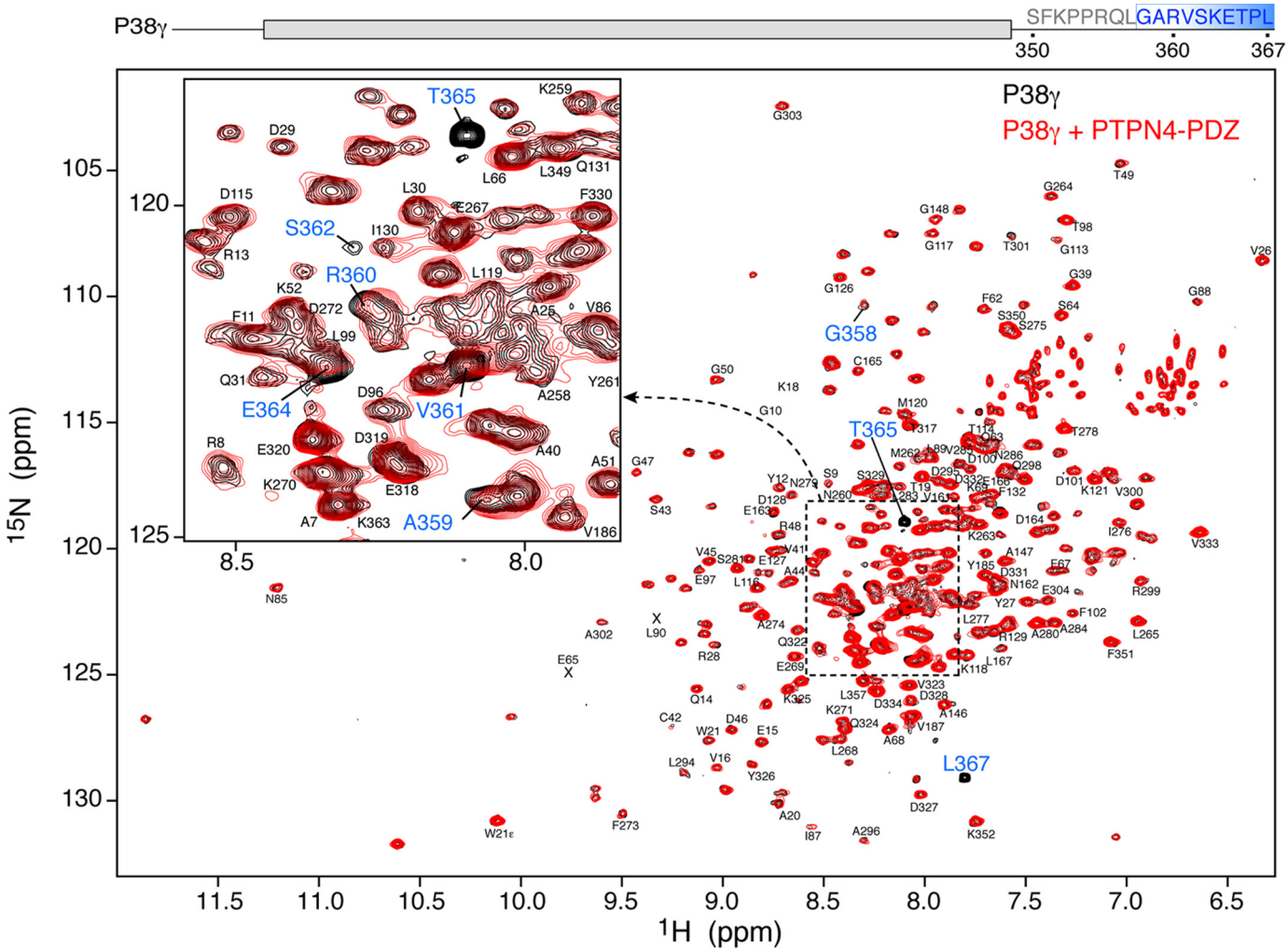

FIGURE 4. **Chemical shift perturbations of p38γ induced by PTPN4-PDZ binding.** Overlay of ^{1}H,^{15}N HSQC spectra recorded on free p38γ (*black*) and on p38γ in complex with PTPN4-PDZ (*red*). Assignment of p38γ is indicated in *black*. The residues perturbed by PTPN4-PDZ binding (labeled in *blue*) are located at the C terminus (Gly-358–Leu-367_{COOH}) and are affected in a gradual manner toward the C terminus as schematically indicated at the *top*.

binds PTPN4-PDZ via its C terminus PBM motif in a conventional PBM·PDZ manner and that no additional p38γ regions are involved in the binding to PTPN4-PDZ as monitored by NMR.

The PBM of p38γ Is the Major Contributor to the PTPN4·p38γ Interaction—We established that p38γ interacts tightly with PTPN4-PDZ via its PBM. Next, we studied the contribution of this PBM·PDZ interaction to the association between the PDZ-PTP^{WT} two-domain of PTPN4 and the full-length p38γ by ITC. We noticed that p38γ-KETPL binds PDZ-PTP^{WT} with an affinity (1.54 ± 0.24 μM) similar to that observed by NMR for PTPN4-PDZ (1.58 ± 0.97 μM). This indicates that the PTP domain does not affect the PDZ ligand binding. Full-length p38γ binds PDZ-PTP^{WT} with an affinity of 4.1 ± 0.3 μM that is slightly higher than the one calculated for the PDZ-PTP^{WT}·p38γ-KETPL association. In both cases, the interactions are mainly driven by an overall enthalpy contribution and with an unfavorable entropic penalty for the full-length p38γ, most likely due to a decrease of conformational freedom of the two proteins in the presence of the kinase domain (Table 2). Then, we investigated the contribution of the PBM recognition on the PDZ-PTP^{WT}·p38γ interaction. The addition of the p38γ-KETPL peptide in large excess (*i.e.* 95% of saturation of the PDZ binding site) abrogates the interaction between PTPN4-PDZ and p38γ (Table 2, Fig. 5). The PBM·PDZ association is, therefore, the major contributor to the PDZ-PTP^{WT}·p38γ interaction. However, a residual heat [$\Delta H \approx -4.1$ kcal·mol^{-1}] was observed at the end of the p38γ titration or during the competition experiment. This enthalpy does not correspond to the heat of dilution (Fig. 5*B*, *inset*). This event could be related to a weak binding of PDZ/PBM off-site, which could involve the phosphatase domain and the kinase domain.

The Inhibition of the Catalytic Activity of PTPN4 by Its PDZ Domain Is Released when the PDZ Binding Site Is Occupied by p38γ-KETPL—We recently demonstrated that the PDZ domain of PTPN4 down-regulates the phosphatase activity through intramolecular interactions and that the mere binding of a PDZ ligand releases this catalytic inhibition (20). Here, we investigated whether the binding of p38γ-KETPL to the PDZ domain could also affect this catalytic regulation and in turn modulate the phosphatase activity. As we previously reported, the PDZ domain inhibits the catalytic activity of PTPN4 through a mixed inhibition. Indeed, the turnover number (k_{cat}) values decreased by 3.3-fold from linker-PTP to PDZ-PTP^{WT},

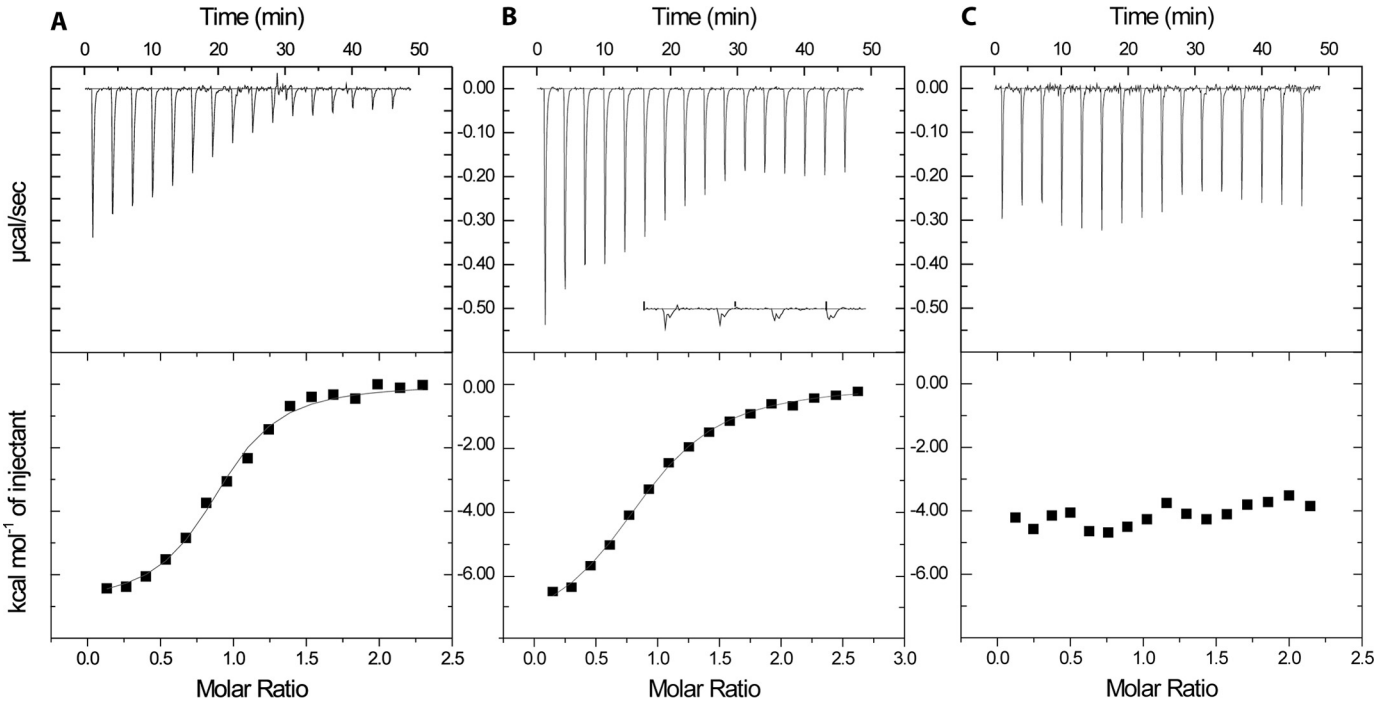

FIGURE 5. **Isothermal calorimetry titrations of PTPN4 PDZ-PTP^{WT} by p38γ-KETPL peptide and full-length p38γ.** Raw isothermal titration calorimetry data (*upper panels*) and derived binding isotherm plotted *versus* the molar ratio of titrant fit using a one-site model (*lower panels*). *A*, PTPN4 PDZ-PTP^{WT} titrated by p38γ-KETPL peptide. *B*, PTPN4 PDZ-PTP^{WT} titrated by full-length p38γ (the *inset* corresponds to the heat of dilution). *C*, PTPN4 PDZ-PTP^{WT} titrated by full-length p38γ in the presence of an excess of the p38γ-KETPL peptide.

whereas the Michaelis constant (K_m) value decreased by a 2.2-fold using *p*-nitrophenyl phosphate as substrate (Table 3). The kinetic analysis of PDZ-PTP^{WT} was then carried out in the presence of p38γ-KETPL peptide at a concentration sufficient enough to ensure the maximal effect of the PDZ ligand on the phosphatase activity. Both the k_{cat} and K_m values significantly increased in the presence of p38γ-KETPL, showing that the release of the inhibition operates with partial compensation of the effect on the two rate constants (Table 3). The k_{cat} and K_m values are 2.3-fold and 2.2-fold higher, respectively, in the presence of p38γ-KETPL. Altogether, these data indicate that the PBM of p38γ has the ability to modulate the phosphatase activity of PTPN4.

In addition, PTPN4 was assessed for its capacity to dephosphorylate the full-length p38γ. To this aim, p38γ was produced and fully phosphorylated on the activation loop (TGpY) using *in vitro* MKK6 kinase. We measured the dephosphorylation of full-length phospho-p38γ by the PTPN4 linker-PTP and PDZ-PTP^{WT} in the presence or absence of an excess of p38γ-KETPL peptide (final concentration 40 μM) at 30 μM phospho-p38γ (Fig. 6*A*). We performed the same experiments with the TGpY peptide as a substrate to compare the activation coming from the presence of the PBM on the full-length p38γ. We observed that the full-length p38γ kinase was efficiently dephosphorylated by PTPN4 linker-PTP and PDZ-PTP^{WT} with or without an excess of p38γ-KETPL peptide (Fig. 6*A*). The initial rates of linker-PTP and PDZ-PTP^{WT} with p38γ-KETPL were similar, whereas the initial rate of PDZ-PTP^{WT} alone was slightly lower (Fig. 6*A*). The relative amplitude between PDZ-PTP^{WT} alone and PDZ-PTP^{WT} with excess of peptide is significantly reduced with the full-length p38γ as a substrate (ratio of initial rates of PDZ-PTP^{WT}+KETPL/PDZ-PTP^{WT} of 1.31) (Fig. 6*A*) compared with the one with the TGpY peptide as a substrate (ratio of 2.60) (Fig. 6*B*). This strongly suggests that the presence of the PBM on the full-length p38γ already releases the inhibition of the PDZ domain of PTPN4 by the PDZ·PBM interaction from the enzyme·substrate complex.

Discussion

PTPN4 functions as an anti-apoptotic protein. The interaction of PTPN4-PDZ with the PBM of cellular partners is critical for the protection of cells against cell death as PBM binding to PTPN4-PDZ jeopardizes cell homeostasis (Refs. 6 and 15 and this study). However, the cellular partners that directly interact with PTPN4 are poorly known. In this study we identified the MAP kinase p38γ as a PTPN4-interacting protein. Both proteins are well expressed in human glioblastoma and neuroblastoma cells and depletion of p38γ or PTPN4, both, lead to cell death. We show that p38γ and PTPN4 interact *in vitro* and in neuroblastoma cell extracts. This interaction is mediated by the PDZ domain of PTPN4 and the PBM of p38γ. The p38γ kinase PBM has the highest affinity among endogenous partners of PTPN4 described up to now with a micromolar affinity for the PDZ domain of PTPN4. Indeed, we previously showed that the C-terminal motifs of two known endogenous partners of PTPN4, the GluN2A subunit of the *N*-methyl-D-aspartate receptor and the GluD2 subunit of the orphan ionotropic glutamate receptor, bind to the PDZ domain of PTPN4 with k_D values equal to 128 μM and 42 μM, respectively (15). The micromolar affinity observed for the association of the PBM of p38γ with PTPN4-PDZ was also previously reached by our optimized PBM peptide, Cyto8-RETEV. This peptide was designed

TABLE 3

Kinetic parameters of the hydrolysis of *p*-nitrophenyl phosphate (*p*NPP) and phosphorylated TGY-p38γ loop by various PTPN4 constructs

The initial reaction rates at each substrate concentration were independently measured at pH 7.5 and 25 °C. The Michaelis constant (K_m) and the turnover number (k_{cat}) values were deduced by fitting the experimental data to the Michaelis-Menten equation. The data and error are representative of three independent experiments.

Substrate	PTPN4 constructs	K_m	k_{cat}	k_{cat}/K_m
		μM	s^{-1}	$s^{-1}.M^{-1}$
*p*NPP	Linker-PTP[a]	640 ± 24	5.0 ± 0.2	7810 ± 380
	PDZ-PTP^{WT}[a]	290 ± 10	1.5 ± 0.1	5170 ± 430
	PDZ-PTP^{WT} + Cyto8-RETEV[a] (40 mM)	690 ± 15	3.8 ± 0.2	5510 ± 170
	PDZ-PTP^{WT} + p38γ-KETPL (40 μM)	640 ± 60	3.5 ± 0.4	5543 ± 628
TGpY	Linker-PTP[a]	16.2 ± 0.2	11.7 ± 0.3	722 E3 ± 20.5
pTGpY	Linker-PTP	4.70 ± 0.5	11.5 ± 0.2	2450 E3 ± 264.0

[a] Data are from Maisonneuve *et al.* (20).

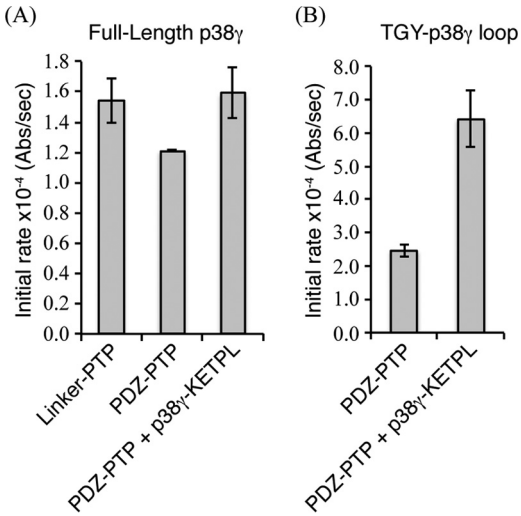

FIGURE 6. **Phosphatase activity of PTPN4 constructs on full-length p38γ and phosphorylated TGY-p38γ loop.** *A*, initial rates of full-length phospho-p38γ dephosphorylation by linker-PTP (10 nM) and by PDZ-PTP^{WT} (10 nM) with 30 μM phospho-p38γ. Values of PDZ-PTP^{WT} were determined in the absence of peptide (*PDZ-PTP*) or in the presence of 40 μM peptide p38γ-KETPL (*PDZ-PTP+p38γ-KETPL*). The data and *error bars* are representative of two independent experiments. *B*, initial rates of phosphorylated TGY-p38γ loop (TGpY) dephosphorylation by PDZ-PTP^{WT} (10 nM) with 30 μM TGpY in the absence of peptide (*PDZ-PTP*) or in the presence of 40 μM peptide p38γ-KETPL (*PDZ-PTP + p38γ-KETPL*).

based on the x-ray structure of the PTPN4-PDZ in complex with a low affinity RABV PBM ligand ($-GETRL_{-COOH}$). Here, our x-ray structural study of PTPN4-PDZ in complex with the C-terminal sequence of p38γ and the tailored peptide Cyto8-RETEV revealed the crucial structural determinants explaining the gain in affinity. Indeed, the two high affinity sequences contract additional interactions between their basic residue at position −4 of the PBM and the Asp-580 of PTPN4-PDZ and are devoid of unfavorable Arg at position −1 surrounded by positively charged residues of PTPN4 observed for the low affinity viral sequence. These common interactions stabilized the complexes and hence explained the high affinity of Cyto8-RETEV and p38γ-KETPL for the PDZ domain of PTPN4.

The C-terminal sequence of p38γ alone is able to mainly recapitulate the thermodynamics properties observed in the full-length p38γ·PTPN4-PDZ-PTP complex as revealed by our isothermal calorimetric titrations. Full-length p38γ binds PTPN4-PDZ via its C terminus PBM motif in a conventional type I PBM·PDZ manner, and no other regions of the kinase are involved in the complex formation, as we did not monitor by NMR any chemical shift perturbation of the kinase domain in the presence of PTPN4-PDZ. The PDZ·PBM interaction is, therefore, the major contributor to the p38γ·PTPN4 complex formation. Among p38 family proteins, p38γ is the only member to encode a C-terminal PBM. This unique feature of this kinase allows its recruitment independently of the presence of a kinase interaction motif identified in nearly every MAPK regulatory and substrate protein (12). Interestingly, the two NT5 tyrosine phosphatase group members, PTPN3 and PTPN4, both, sharing the same domains organization, take advantage of this unique feature to recruit p38γ through their PDZ domain (12). Thus, the recognition of the PBM of p38γ by the PDZ domain of PTPs greatly contributes to the specificity of the interaction compared with other MAPK proteins.

In addition, our results show that recruitment of the PBM of p38γ by the PTPN4 PDZ domain has a further functional consequence. The catalytic activity of both PTPN4 and PTPN3 is autoinhibited by their PDZ domain when the PDZ and PTP two-domain adopt a compact conformation (20, 30). We demonstrate here that the binding of the PBM of p38γ to PTPN4-PDZ lifts this inhibition and restores the PTPN4 phosphatase activity. We previously described that the PBM binding to the PDZ likely causes partial disruption of the transient interactions between the PDZ and PTP domains and the dynamic rearrangement between the two domains, resulting in the activation of the phosphatase. In the PTPN4·p38γ complex, the PDZ domain of PTPN4 is not only crucial in the recruitment of the kinase, but it would also be involved in the control of the phosphatase activity and specifically favors the dephosphorylation of p38γ. After the first PDZ·PBM recognition step, the subsequent phosphatase activation could then serve to induce the dephosphorylation of the TGY activation loop of p38γ, that is crucial for the regulation of the kinase activity.

Viral proteins efficiently mimic cellular PBM such as the one of p38γ, affecting both the recruitment of substrate and the regulation of the activity in the case of PTPN4. Infection by an attenuated RABV strain perturbs the anti-apoptotic function of PTPN4 and induces cell death. The targeting of the PDZ domain of PTPN4 by the PBM of the viral G protein of the attenuated RABV strain, Cyto13-att, abrogates the protective role of PTPN4 and is responsible for the cell death caused by this RABV strain. Nevertheless, the G protein of attenuated RABV strain competes with an endogenous ligand whose identity is not yet known. The PTPN4·p38γ association could be affected by the G protein during viral affection. The mere disturbing of the crucial PDZ·PBM p38γ recruitment step might be sufficient to prevent the dephosphorylation of the kinase and thereby to disrupt its function. Thus, hijacking the

p38γ·PTPN4 signaling by the RABV G protein could be the main cause of the apoptosis phenotype of the attenuated RABV strain. Further studies are necessary to demonstrate this point.

As shown by a few studies such as those of the HtrA2 and DegS proteases and ours on PTPN4 phosphatase, the PDZ domains and their ligand play an essential role in regulating enzymatic activity. Targeting PDZ·PBM interactions involving signaling proteins such as kinases and phosphatases is a promising therapeutic strategy to specifically perturb the homeostasis of tumor cells. By elucidating the molecular basis of PTPN4·p38γ interaction, we are rationally designing new tumoricid molecules inhibiting the phosphatase by locking PDZ and PTP domains together.

Author Contributions—P. M., C. C.-S., B. R., M. L., F. C., and N. W. planned the experiments. P. M., C. C.-S., E. B.-Z., K. S., B. R., M. L., F. C., A. H., and N. W. performed the experiments. P. M., C. C.-S., M.-C. V., E. B.-Z., B. R., M. L., F. C., A. H., and N. W. analyzed the data. P. M., C. C.-S., M.-C. V., M. L., M. D., F. C., and N. W. wrote the paper.

Acknowledgments—We thank M. Lafage (Viral Neuro-Immunology Unit, Institut Pasteur), P. England, S. Hoos (Proteopole, Institut Pasteur), C. Malosse (Structural Mass Spectrometry and Proteomics Unit), and C. Simenel (NMR unit, Institut Pasteur) for technical expertise. We thank E. Lescop for NMR technical expertise and helpful discussions (ICSN, Gif/Yvette, France). We thank the staff from the Protein Crystallization platform at the Institut Pasteur and the staff of the PROXIMA-1 beamline at the SOLEIL synchrotron (St Aubin, France).

References

1. Kina, S.-i., Tezuka, T., Kusakawa, S., Kishimoto, Y., Kakizawa, S., Hashimoto, K., Ohsugi, M., Kiyama, Y., Horai, R., Sudo, K., Kakuta, S., Iwakura, Y., Iino, M., Kano, M., Manabe, T., and Yamamoto, T. (2007) Involvement of protein-tyrosine phosphatase PTPMEG in motor learning and cerebellar long-term depression. *Eur. J. Neurosci.* **26,** 2269–2278
2. Kohda, K., Kakegawa, W., Matsuda, S., Yamamoto, T., Hirano, H., and Yuzaki, M. (2013) The δ2 glutamate receptor gates long-term depression by coordinating interactions between two AMPA receptor phosphorylation sites. *Proc. Natl. Acad. Sci. U.S.A.* **110,** e948–e957
3. Young, J. A., Becker, A. M., Medeiros, J. J., Shapiro, V. S., Wang, A., Farrar, J. D., Quill, T. A., Hooft van Huijsduijnen, R., and van Oers, N. S. (2008) The protein tyrosine phosphatase PTPN4/PTP-MEG1, an enzyme capable of dephosphorylating the TCR ITAMs and regulating NF-kappaB, is dispensable for T cell development and/or T cell effector functions. *Mol. Immunol.* **45,** 3756–3766
4. Gu, M., Meng, K., and Majerus, P. W. (1996) The effect of overexpression of the protein tyrosine phosphatase PTPMEG on cell growth and on colony formation in soft agar in COS-7 cells. *Proc. Natl. Acad. Sci. U.S.A.* **93,** 12980–12985
5. Zhou, J., Wan, B., Shan, J., Shi, H., Li, Y., and Huo, K. (2013) PTPN4 negatively regulates CrkI in human cell lines. *Cell Mol. Biol. Lett.* **18,** 297–314
6. Préhaud, C., Wolff, N., Terrien, E., Lafage, M., Mégret, F., Babault, N., Cordier, F., Tan, G. S., Maitrepierre, E., Ménager, P., Chopy, D., Hoos, S., England, P., Delepierre, M., Schnell, M. J., Buc, H., and Lafon, M. (2010) Attenuation of rabies virulence: takeover by the cytoplasmic domain of its envelope protein. *Sci. Signal.* **3,** ra5
7. Gu, M., and Majerus, P. W. (1996) The properties of the protein tyrosine phosphatase PTPMEG. *J. Biol. Chem.* **271,** 27751–27759
8. Harris, B. Z., and Lim, W. A. (2001) Mechanism and role of PDZ domains in signaling complex assembly. *J. Cell Sci.* **114,** 3219–3231
9. Lee, H.-J., and Zheng, J. J. (2010) PDZ domains and their binding partners: structure, specificity, and modification. *Cell Commun. SignaL.* **8,** 8
10. Yanagisawa, J., Takahashi, M., Kanki, H., Yano-Yanagisawa, H., Tazunoki, T., Sawa, E., Nishitoba, T., Kamishohara, M., Kobayashi, E., Kataoka, S., and Sato, T. (1997) The molecular interaction of Fas and FAP-1: a tripeptide bloker of human Fas interaction with FAP-1 promotes Fas-induced apoptosis. *J. Biol. Chem.* **272,** 8539–8545
11. Aarts, M., Liu, Y., Liu, L., Besshoh, S., Arundine, M., Gurd, J. W., Wang, Y.-T., Salter, M. W., and Tymianski, M. (2002) Treatment of ischemic brain damage by perturbing NMDA receptor-PSD-95 protein interactions. *Science* **298,** 846–850
12. Hou, S.-W., Zhi, H.-Y., Pohl, N., Loesch, M., Qi, X.-M., Li, R.-S., Basir, Z., and Chen, G. (2010) PTPH1 dephosphorylates and cooperates with p38γ MAPK to increase ras oncogenesis through PDZ-mediated interaction. *Cancer Res.* **70,** 2901–2910
13. Caillet-Saguy, C., Maisonneuve, P., Delhommel, F., Terrien, E., Babault, N., Lafon, M., Cordier, F., and Wolff, N. (2015) Strategies to interfere with PDZ-mediated interactions in neurons: what we can learn from the rabies virus. *Prog. Biophys. Mol. Biol.* **119,** 53–59
14. Chen, V. B., Arendall, W. B., 3rd, Headd, J. J., Keedy, D. A., Immormino, R. M., Kapral, G. J., Murray, L. W., Richardson, J. S., and Richardson, D. C. (2010) *MolProbity*: all-atom structure validation for macromolecular crystallography. *Acta Crystallogr. D Biol. Crystallogr.* **66,** 12–21
15. Babault, N., Cordier, F., Lafage, M., Cockburn, J., Haouz, A., Prehaud, C., Rey, F. A., Delepierre, M., Buc, H., Lafon, M., and Wolff, N. (2011) Peptides targeting the PDZ domain of PTPN4 are efficient inducers of glioblastoma cell death. *Structure* **19,** 1518–1524
16. Hironaka, K., Umemori, H., Tezuka, T., Mishina, M., and Yamamoto, T. (2000) The protein-tyrosine phosphatase PTPMEG interacts with glutamate receptor δ2 and ε subunits. *J. Biol. Chem.* **275,** 16167–16173
17. Huai, W., Song, H., Wang, L., Li, B., Zhao, J., Han, L., Gao, C., Jiang, G., Zhang, L., and Zhao, W. (2015) Phosphatase PTPN4 preferentially inhibits TRIF-dependent TLR4 pathway by dephosphorylating TRAM. *J. Immunol.* **194,** 4458–4465
18. Raman, M., Chen, W., and Cobb, M. H. (2007) Differential regulation and properties of MAPKs. *Oncogene* **26,** 3100–3112
19. Kukkonen-Macchi, A., Sicora, O., Kaczynska, K., Oetken-Lindholm, C., Pouwels, J., Laine, L., and Kallio, M. J. (2011) Loss of p38γ MAPK induces pleiotropic mitotic defects and massive cell death. *J. Cell Sci.* **124,** 216–227
20. Maisonneuve, P., Caillet-Saguy, C., Raynal, B., Gilquin, B., Chaffotte, A., Pérez, J., Zinn-Justin, S., Delepierre, M., Buc, H., Cordier, F., and Wolff, N. (2014) Regulation of the catalytic activity of the human phosphatase PTPN4 by its PDZ domain. *FEBS J.* **281,** 4852–4865
21. Kabsch, W. (2010) *XDS*. *Acta Crystallogr. D Biol. Crystallogr.* **66, 125–132**
22. Evans, P. R., and Murshudov, G. N. (2013) How good are my data and what is the resolution? *Acta Crystallogr. D Biol. Crystallogr.* **69,** 1204–1214
23. Winn, M. D., Ballard, C. C., Cowtan, K. D., Dodson, E. J., Emsley, P., Evans, P. R., Keegan, R. M., Krissinel, E. B., Leslie, A. G., McCoy, A., McNicholas, S. J., Murshudov, G. N., Pannu, N. S., Potterton, E. A., Powell, H. R., Read, R. J., Vagin, A., and Wilson, K. S. (2011) Overview of the CCP4 suite and current developments. *Acta Crystallogr. D* **67,** 235–242
24. McCoy, A. J. (2007) Solving structures of protein complexes by molecular replacement with Phaser. *Acta Crystallogr. D* **63,** 32–41
25. Emsley, P., and Cowtan, K. (2004) Coot: model-building tools for molecular graphics. *Acta Crystallogr. D* **60,** 2126–2132
26. Blanc, E., Roversi, P., Vonrhein, C., Flensburg, C., Lea, S. M., and Bricogne, G. (2004) Refinement of severely incomplete structures with maximum likelihood in BUSTER-TNT. *Acta Crystallogr. D* **60,** 2210–2221
27. Lovell, S. C., Davis, I. W., Arendall, W. B., 3rd, de Bakker, P. I., Word, J. M., Prisant, M. G., Richardson, J. S., and Richardson, D. C. (2003) Structure validation by Cα geometry: ϕ, ψ, and Cβ deviation. *Proteins* **50,** 437–450
28. Vogtherr, M., Saxena, K., Grimme, S., Betz, M., Schieborr, U., Pescatore, B., Langer, T., and Schwalbe, H. (2005) NMR backbone assignment of the mitogen-activated protein (MAP) kinase p38. *J. Biomol. NMR* **32,** 175
29. Francis DM, Róycki B, Koveal D, Hummer G, Page R, Peti W. (2011) Structural basis of p38α regulation by hematopoietic tyrosine phosphatase. *Nat Chem Biol.* **7,** 916–924
30. Chen, K.-E., Lin, S.-Y., Wu, M.-J., Ho, M.-R., Santhanam, A., Chou, C.-C., Meng, T.-C., and Wang, A. H. (2014) Reciprocal allosteric regulation of p38 and PTPN3 involves a PDZ domain-modulated complex formation. *Sci. Signal.* **7,** ra98

Molecular Basis of the Interaction of the Human Protein Tyrosine Phosphatase Non-receptor Type 4 (PTPN4) with the Mitogen-activated Protein Kinase p38 γ

Pierre Maisonneuve, Célia Caillet-Saguy, Marie-Christine Vaney, Edoo Bibi-Zainab, Kristi Sawyer, Bertrand Raynal, Ahmed Haouz, Muriel Delepierre, Monique Lafon, Florence Cordier and Nicolas Wolff

J. Biol. Chem. 2016, 291:16699-16708.
doi: 10.1074/jbc.M115.707208 originally published online May 31, 2016
